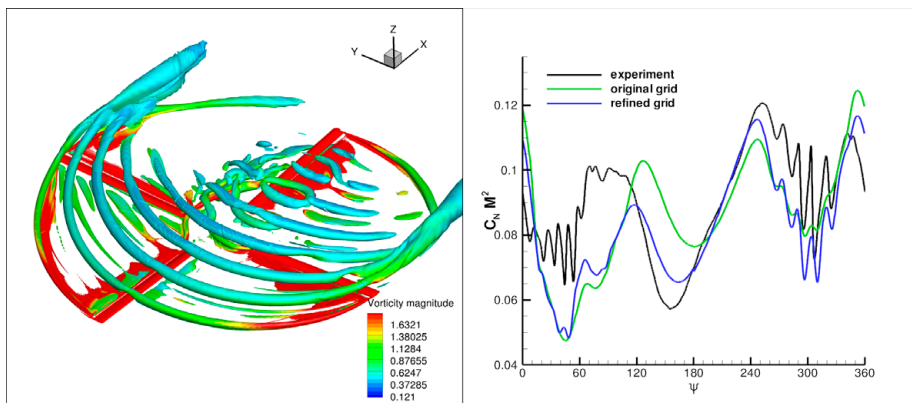




Executive summary

Simulation of a rotor in forward flight using topology-based refinement of multi-block structured meshes



Report no.

NLR-TP-2012-485

Author(s)

H. van der Ven
O.J. Boelens
J.C. Kok
B.B. Prananta
M.P.C. van Rooij

Report classification

UNCLASSIFIED

Date

January 2013

Knowledge area(s)

Computational Physics en
theoretische aërodynamica
Helikoptertechnologie

Descriptor(s)

CFD
local refinement
BVI
simulation
higher order

Problem area

Maintenance of helicopters is complicated by the high levels of vibrations in the fuselage. The vibrations are mainly caused by the vibrations that are passed by the blades through the rotor hub. Part of the blade vibrations are induced by blade-vortex interactions: the blades fly in each other's wake and the tip vortices interact with the blade, causing possibly strong pressure fluctuations.

The prediction of the blade-vortex interactions is one of the grand challenges of computational fluid dynamics. Standard numerical methods will dissipate the tip vortices long before they interact with the following blades. For accurate prediction of the interactions, the vortices should be

resolved for at least one and a half rotor revolution, which is a distance of about one hundred blade chords. Numerical techniques which may predict blade-vortex interactions, combine higher-order methods with grid refinement.

Description of work

The high-order finite volume flow solver ENSOLV is extended with the capability to accommodate grids where at block interfaces mesh ratios of two to one or higher exist. For such grids, high resolution in localised regions can be obtained without outward radiation of the grid density. Hence such grids can be used to obtain a uniform resolution in the helicopter rotor disk area, required to resolve the tip vortices. The generation of such meshes is, however, not straightforward and

This report is based on a presentation held at the 38th European Rotorcraft Forum, Amsterdam, the Netherlands, September 4-6, 2012.

The current version is an extended version with respect to the version published in the proceedings of the forum.

may involve a significant amount of user interaction. In order to avoid this, a new multi-block structured grid generation algorithm is developed which automatically refines an existing block topology to accommodate a mesh with uniform and high resolution in the rotor disk area.

The grid generation algorithm is applied to the HART-II rotor experiment, which is one of the most widely-used comprehensive databases for validation of CFD algorithms for helicopter flow.

Results

Starting from a standard multiblock structured grid around the BO105 rotor blades with 13 million cells, a locally refined mesh is automatically generated with a resolution of one percent rotor radius in the rotor disk.

The new mesh has 26 million elements.

Trimmed aero-elastic simulations using the fourth-order accurate finite volume scheme have been performed on both meshes. The vortex resolution on the refined mesh improves considerably with respect to the original mesh. On the retreating side, blade-vortex interactions are evident from the blade aero- dynamic forces. Comparison with experiment shows that the grid resolution is not yet sufficient to predict all blade-vortex interactions. This is in accordance with results from literature.

Applicability

The new grid generation algorithm can be applied to any flow problem where localised flow features are important.



NLR-TP-2012-485

Simulation of a rotor in forward flight using topology-based refinement of multi-block structured meshes

H. van der Ven, O.J. Boelens, J.C. Kok, B.B. Prananta and
M.P.C. van Rooij

This report is based on a presentation held at the 38th European Rotorcraft Forum, Amsterdam, the Netherlands, September 4-6, 2012.




The current version is an extended version with respect to the version published in the proceedings of the forum.

The contents of this report may be cited on condition that full credit is given to NLR and the authors.

This publication has been refereed by the Advisory Committee AEROSPACE VEHICLES.

Customer National Aerospace Laboratory NLR
Contract number ---
Owner NLR
Division NLR Aerospace Vehicles
Distribution Unlimited
Classification of title Unclassified
 January 2013

Approved by:

Author H. van der Ven 	Reviewer M.P.C. van Rooij 	Managing department K. de Cock 
Date: 2013/1/24	Date: 2013/01/24	Date: 25/1/2013

Contents

Summary	4
1 Introduction	7
2 Topology-based block-refinement algorithm	8
2.1 Grid generation algorithm	8
2.2 Discretization scheme on irregular block interfaces	9
3 Results	10
3.1 Grid	10
3.2 Rigid-blade trim	10
3.3 Aeroelastic trim	11
3.4 Flow results	12
4 Conclusions	13
References	15

Summary

The simulation of blade-vortex interaction (BVI) for helicopter rotors remains a challenge for Computational Fluid Dynamics (CFD). In the current paper a high-order, block-structured, finite volume flow solver is applied to the well-known HART-II baseline case. A new grid generation algorithm is presented which allows the automatic generation of locally refined meshes in user-specified regions, based on a regular block-structured mesh. The algorithm is used to generate a mesh with a given uniform resolution in the rotor disk area. The convection of the tip vortices is expected to improve on such a mesh. Flow results on both the unrefined and refined mesh confirm this expectation.

Symbols and abbreviations

BVI	Blade-Vortex Interaction
CFD	Computational Fluid Dynamics
NLR	National Aerospace Laboratory
R	rotor radius
$C_N M^2$	normal force coefficient $C_N M^2 = \frac{N}{\frac{1}{2} \rho_\infty a_\infty^2 A}$
N	normal force [N]
ρ_∞	atmospheric air density [kg/m ³]
a_∞	atmospheric speed of sound [m/s]
A	reference area [m ²]
θ_0	collective pitch [°]
θ_{1c}	longitudinal cyclic pitch [°]
θ_{1s}	lateral cyclic pitch [°]
ψ	azimuth angle [°]
Q	Q-criterion: $\Omega^2 - S^2$ [s ⁻²]
S	magnitude of strain rate tensor [s ⁻¹]
U_∞	forward rotor speed [m/s]
Ω	magnitude of vorticity [s ⁻¹]



This page is intentionally left blank.

1 Introduction

In level helicopter flight there are two regimes with high vibration levels, low speed transition flight and high speed forward flight. The two high vibration regimes translate directly into high operating and maintenance costs. There are three key aerodynamic phenomena which contribute to the vibratory loads: wake induced air loads, compressibility effects, and dynamic stall. The current paper focuses on the accurate resolution of wake-induced air loads using Computational Fluid Dynamics (CFD) techniques.

As summarised in Datta et al. (Ref. 1), first principles CFD calculation of the wake is primarily a grid refinement problem. In order to capture the tip vortices the computational mesh must be refined in the vortex regions, which are not known beforehand. The dynamic nature of the wake in forward flight complicates the refinement problem since the vortices change position over time.

With the increase in computing power, there is a tendency in the CFD community to apply simple high-order finite difference schemes on dense Cartesian background meshes and standard second-order finite volume schemes in the neighbourhood of the geometry (Jayaraman et al. Ref. 2 and Sankaran et al. Ref. 5). While this method shows impressive vortex capturing capabilities on the background mesh, it has two drawbacks: 1) the numerics are only second order in the proximity of the rotor blades; 2) the Chimera approach requires interpolation of the flow solution between the two types of grid.

At NLR a high-order, block-structured, finite volume flow solver has been developed which maintains its high order of accuracy in the whole of the computational domain (Kok Ref. 4). The main challenge in applying this solver to rotor flow is to obtain a grid resolution similar to the resolution of the background grid used in Ref. 2, 5. Geometrical and topological restrictions normally prevent the generation of a block-structured grid which has a uniform resolution in the rotor wake.

Note that within a block-structured framework, local cell-based refinement of the mesh is not possible as this will destroy the block structure of the mesh. Since the extension of the flow solver to unstructured meshes is an unfeasibly large task, the current paper focuses on the generation of efficient meshes which are block-structured.

A topology-based refinement scheme is presented which allows the generation of such meshes. In the approach, the block topology is refined in such a way that a uniform mesh can be obtained locally without outward radiation of the grid density. This is achieved at a cost: at block

boundaries the grid may be irregular. Mesh width ratio's of 2:1 or higher may be present. However, since the block boundaries are still conforming it is possible to devise high-order accurate schemes across such boundaries.

The outline of the report is as follows. Section 2 describes the refinement algorithm for the generation of the appropriate meshes and the discretization scheme on the irregular block interfaces. Section 3 describes the refined mesh for the HART II test case and the simulation results for the refined and unrefined mesh. Finally, in Section 4 conclusions are drawn.

2 Topology-based block-refinement algorithm

2.1 Grid generation algorithm

The multi-block flow solver ENSOLV at NLR allows block-wise refinement of the mesh, where the grid in a block is refined in one or more direction(s). The resulting irregularities at block interfaces, where the ratio of mesh widths may be $2^n:1$, can be treated by the finite-volume flow solver in an accurate way. Block-wise refined meshes have the potential of attaining uniform grid spacing in the vortex regions. However, the grids may not be that efficient, since the grid resolution may be too small in some regions. This may happen inside the vortex region for a block with significant stretching: if the coarse cells satisfy the resolution requirement, the fine cells will be too small. It may also happen outside the vortex region when the refined block is only partially contained in the vortex region. These examples show that an efficient grid with block-wise refinement can only be obtained if the topology of the mesh is modified.

The new topology-based grid generation algorithm is described briefly below. The interested reader may find more details in Van der Ven et al.(Ref. 6). The algorithm consists of the following steps:

1. uniform refinement of the block topology to a fixed block size (measured as the number of cells within a block); typically the target block size is 8^3 or 16^3 ;
2. further topology-refinement of those blocks which are targeted for grid refinement; the subblock topology is such that each grid-refined subblock is as close as possible to the fixed block size used in step 1;
3. based on the user-defined maximum grid irregularity (2:1, 4:1, etc.) blocks bounding the refinement region are targeted for refinement, and step 2 is repeated for those blocks;
4. generate the block grids within the refined topology.

In step 2 a refinement sensor is used which indicates how the grid within a block should be refined. The sensor consists of two parts: 1) the target mesh width; 2) the region where this mesh

width should be attained. The target mesh width should be attained for all cells within a block. The refinement region can be specified in different ways:

- distance to a geometric object;
- specification of specific blocks;
- a region described by a simple geometric object such as a sphere, cylinder, or cube.

As the aim of the topology refinement is a uniform mesh, the grid refinement within a block can be anisotropic.

The algorithm is demonstrated for the NACA0012, using a refinement region defined by the distance to a line segment. This example serves as an illustration of the algorithm only, in Section 3.1 the algorithm will be applied to the isolated BO105 rotor.

The original mesh and topology is shown in Figure 1a. With a specified block size of 8^2 , the refined topology of step 1 of the algorithm is shown in Figure 1b. The line segment used to define the refinement region is shown in Figure 1c. A region at a distance of 10% chord to this segment is defined as the refinement region. Within this region a mesh width of 0.001 chord should be attained. Figure 1d shows the refined topology which is the result of step 2 of the algorithm. Note that at this stage the grid has not been refined yet and that some of the blocks in the refined topology consist of a single cell of the original mesh.

Subsequently, the user-defined irregularity is applied. Figure 1e shows the refined topology based on a maximum irregularity of 2:1. In the last step of the algorithm the refined grid is generated, which is shown in Figure 1f.

It is worthy to note that the final topology consists of 982 blocks. Clearly, it is unfeasible to expect from a user to generate such topologies by hand.

2.2 Discretization scheme on irregular block interfaces

At the irregular block interfaces the standard numerical scheme cannot be applied since the cell-centered flow data is not available at the other side of the interface. The flow data is interpolated to the required location in planes parallel to the interface, as shown in Figure 2. The interpolation is performed in computational space, that is, the actual mesh widths are not used as weights in the interpolation, but the weights shown in the figure are used. This is in agreement with the underlying high-order scheme. It should be noted that normal to the interface no interpolation takes place: the planes are considered to be at the right location. This obviously is a crude approximation, but in practice the algorithm is robust, and vortices pass through the interface relatively undisturbed, provided the coarse grid resolution is sufficient.

3 Results

In this chapter, simulations are performed for an isolated four-bladed rotor in one of the flow conditions of the HART-II experiment. The HART-II experiment is described in detail in Van der Wall et al. (Ref. 7). The chosen flow condition is a slow descent flight where multiple BVI events take place during a rotor revolution. The rotor radius of the windtunnel model is 2 meters. Rotational frequency is 109.12 rad/s. Forward speed of the rotor is 32.9 m/s. Effective shaft angle is 4.5 degrees (tilted backward).

3.1 Grid

For rotor flows the convection of the tip vortices in the wake of the blades is important for the capture of the blade-vortex interaction. As the vortices move through the wake, the easiest way of obtaining a mesh with sufficient resolution in the vortex regions is to uniformly refine the mesh in a cylinder around the rotor blades. So the definition of the refinement region in this case is a cylinder centred at the rotor hub with radius equal to the rotor radius and sufficient height to contain the vortices.

The target mesh width is $0.01R$, where R is the rotor radius. This corresponds to 16% chord, which is on the coarse side.

The original mesh has 13 million cells, the refined mesh has 26 million cells. Figure 3a shows a detail of the original mesh in a horizontal plane through the hub. The same detail of the refined mesh is shown in Figure 3b. The uniform resolution in the wake is clearly visible. The imposed grid regularity of 2:1 is also visible in the resolution outside the rotor disk. Figure 4 shows the refinement in a vertical plane through the hub bisecting the rotor disk between two blades.

Figure 5 demonstrates that the target mesh width is actually obtained in the specified refinement region. The figure shows the ratio of the maximum mesh width in a cell over the target mesh width. As can be seen the ratio is less than one in the refinement region, demonstrating the correct functioning of the algorithm. The figure also shows that the algorithm is relatively efficient: the region where the target mesh width is attained is not that much bigger than the refinement region.

3.2 Rigid-blade trim

As a pre-cursor computation the rotor is trimmed with rigid blades. The rotor has been trimmed to the experimental values of thrust, rolling moment, and pitching moment. The trim results are tabulated in Table 1. The obtained thrust is 10% higher than the experimental thrust. As the main

objective of the this simulation is to investigate the effect of local grid refinement, and not comparison with experiment, the trim is not pursued to higher accuracy. At these trim conditions there is evidence of BVI on the retreating side, so the conditions are sufficient for the current investigation.

3.3 Aeroelastic trim

To account for the effects of blade flexibility to the trim, mutual interaction between blade aerodynamics and structural dynamics is modelled by solving the aeroelastic equations in modal space. The aeroelastic deformations are expressed in a limited degrees-of-freedom model built upon the vibration modes of the rotating blade. The required modal data, that is, the natural frequencies and vibrations modes, are computed with respect to the deformed shape due to centrifugal loads. This means that the deformation is linearized around this deformed shape, see Figure 6.

The structural dynamics of the blade is represented using a finite element modelling. A NAS-TRAN model of the blade is generated based on the available elasto-mechanical properties reported in the documentation of the HARTII experiment (Ref. 7). First, static deformation of the blade is determined using a nonlinear approach. Subsequently normal mode analysis is carried out starting from this deformed shape, taking into account the effects of the centrifugal force in the stiffness matrix. The natural frequencies of the blade at various rotational speeds are shown in Figure 7. Measured frequencies at zero rotational speed and computed frequencies using CAMRAD at the reference rotational speed are also presented. Good agreement with both data is observed. Hence, no attempts have been made to improve the correlation by model-updating.

During the simulations on the original grid it became clear that the response of the first lead-lag mode (at a frequency of 0.64/rev) was hardly damped by the aerodynamic forces. As the corresponding period of the mode is almost one-and-a-half revolution, the coupled fluid-structure problem displayed a period of three revolutions. From period to period the response was damped a little bit, as can be seen in the first eight revolutions of the response plotted in Figure 8. To resolve the issue, this mode was damped in the structural model, and a periodic solution of the fluid-structure problem was quickly obtained (see the next four revolutions in Figure 8). The trim values are tabulated in Table 1.

Subsequently the flow results were interpolated onto the refined mesh and the simulation continued with the same trim settings. As can be seen from the next five revolutions in Figure 8, the structural response did not change significantly. The aerodynamic forces, however, deviated from the experimental values. Hence, the rotor was retrimmed, to the control angles shown in Table 1

model	grid	θ_0	θ_{1c}	θ_{1s}	thrust [N]	roll mom-ent [Nm]	pitch mom-ent [Nm]
experiment	–	3.8°	1.94°	−1.34°	3300	20	−20
rigid blades	original	3.07°	1.92°	−1.61°	3630	30	−6
flexible blades	original	4.9°	1.7°	−0.15°	3350	42	−24
flexible blades	refined	4.4°	1.3°	−0.15°	3265	4	−14

Table 1 Trim values for the simulations

in order to obtain the correct aerodynamic forces. As can be seen in the last five revolutions in Figure 8, the response from the first flap mode changed significantly, and obviously this can have a definite impact on the miss distance between blades and vortices.

3.4 Flow results

The turbulent flow is modeled using the Reynolds-averaged Navier-Stokes equations with the TNT k - ω turbulence model (Ref. 3). All simulations have been run using the fourth-order accurate finite volume scheme (Ref. 4). Simulations have been performed on the original mesh of 13 million elements, and the locally refined mesh of 26 million elements (see Section 3.1 for details). The time step corresponds to 0.5° azimuth for all simulations.

First the rigid blade results are shown. As the blades are assumed rigid, no comparison is made with experiment, which has elastic blades. Rather, the capability of the refined mesh to better represent the vortices will be demonstrated. Figure 9 shows the instantaneous iso-contour of the Q -criterion for the original mesh. The Q -criterion distinguishes flow under shear stress from rotational flow, and is used here to focus on the tip vortices rather than on the boundary layer vorticity. The value of Q is equal to $0.72(U_\infty/R)^2$; the vorticity is scaled with $2U_\infty/R$. Figure 10 shows the instantaneous iso-contour of the Q -criterion for the refined mesh at the same values of Q and vorticity. The increase in vortex resolution is evident. Hence, the local grid refinement performs as expected.

Continuing with the simulation using flexible blades, the instantaneous iso-contour of the Q -criterion is shown on the refined mesh for the trimmed solution in Figure 11. Compared to the simulation on the original grid, the lift of the blades on the advancing side (azimuth angle between 90 and 180 degrees) is smaller (cf. Figure 12). Hence the strength of the tip vortex shed in this quadrant is less. In order to visualise the vortex system the value of Q is reduced by a factor of two with respect to the previous figures.

The sectional vertical force coefficient at 87% for the two simulations with flexible is shown in Figure 12. The reference area for the force coefficient is equal to the blade chord times the width of the blade section (which consists of the grid faces on the blade intersected by the 87% span plane).

First, the global behaviour of the force history is discussed. The simulation on the original grid generally agrees with the experiment on the retreating side (azimuth angles greater than 200 degrees). On the advancing side the agreement is less than satisfactory. The retrim on the refined mesh improves the agreement with experiment for azimuth angles greater than 120 degrees, but for smaller angles no improvement is seen. This suggests that the blade motion in the simulation is different from the experiment, especially since the control angles of simulation and experiment are different (see Table 1). However, comparing the simulation results with the results of Jayaraman et al. (Ref. 2) suggests otherwise. Figure 13 shows their results combined with the results of the current paper. The control angles in the simulations of Jayaraman match very well with the experimental values. The global behaviour of the sectional lift for all simulations (current and Jayaraman's) is generally the same, especially for the BVI regions on both advancing and retreating side. It should be noted that in the experiment the blades are not structurally the same, due to instrumentation (see the HARTII experimental database). If this explains the differences between simulation and experiment is not sure.

Second, the prediction of BVI is discussed. Comparing the results for the original and refined grid, the increase in vortex resolution on the refined grid is evident from several blade-vortex interactions on the retreating blade. Comparing the refined grid simulation with the experiment, the number of BVI on the retreating side are the same for simulation and experiment. The amplitude of the interactions in the simulation is only half that of the experiment. Comparing with the simulations of Jayaraman in Figure 13 the phase of the BVI are remarkably the same. On the advancing side the current simulation shows almost no evidence of BVI. The simulations of Jayaraman do exhibit BVI on the advancing side. As their mesh has a background resolution of 10% chord, the most plausible explanation of the lack of BVI on the advancing side in the current simulations is lack of resolution.

4 Conclusions

A new grid generation algorithm for block-refined structured meshes has been presented. The algorithm has been applied to generate a mesh around the HART-II rotor which has uniform resolution in the rotor wake. In the simulations, the rotor has been trimmed to the experimental conditions. Simulation results are compared for simulation on the unrefined and refined mesh.

The uniform resolution of the refined mesh in the rotor wake improves the resolution of the tip vortices. As a consequence, the prediction of the BVI phenomenon on the retreating side has improved, compared to the simulation on the unrefined mesh. On the advancing side the resolution of the mesh is insufficient to capture BVI. In the near future, simulations will be performed on more refined meshes.

Acknowledgements

The work described in this paper is partially funded by the EU FP7 IDIHOM project and partially by NLR's programmatic research 'Kennis als Vermogen'.

References

1. A. Datta, M. Nixon, and I. Chopra. Review of rotor loads prediction with the emergence of rotorcraft CFD. *J. of the American Helicopter Society*, 52 (4):287–317, 2007.
2. B. Jayaraman, A.M. Wissink, J.W. Lim, M. Potsdam, and A.C.B. Dimanlig. Helios prediction of blade-vortex interaction and wake of the HART II rotor. Technical Report 2012-0714, AIAA, 2012.
3. J. C. Kok. Resolving the dependence on freestream values for the $k-\omega$ turbulence model. *AIAA Journal*, 38(7):1292–1294, 2000.
4. J.C. Kok. A high-order low-dispersion symmetry-preserving finite-volume method for compressible flow on curvilinear grids. *J. Comput. Phys.*, 228:6811–6832, 2009.
5. V. Sankaran, J. Sitaraman, A. Wissink, A. Datta, B. Jayaraman, M. Potsdam, D. Mavripilis, D. O’RBrien, H. Saberi, R. Cheng, N. Hariharan, and R. Strawn. Application of the helios computational platform to rotorcraft flowfields. Technical Report 2010-1230, AIAA, 2010.
6. H. van der Ven and J.C. Kok. Description and verification of the topology-based block-refinement algorithm. Technical Report CR-2012-571, NLR, 2012.
7. B.G. van der Wall. 2nd HCC aeroacoustics rotor test (HART II) Part I: Test documentation. Technical Report IB 111-2003/19, DLR, 2003.

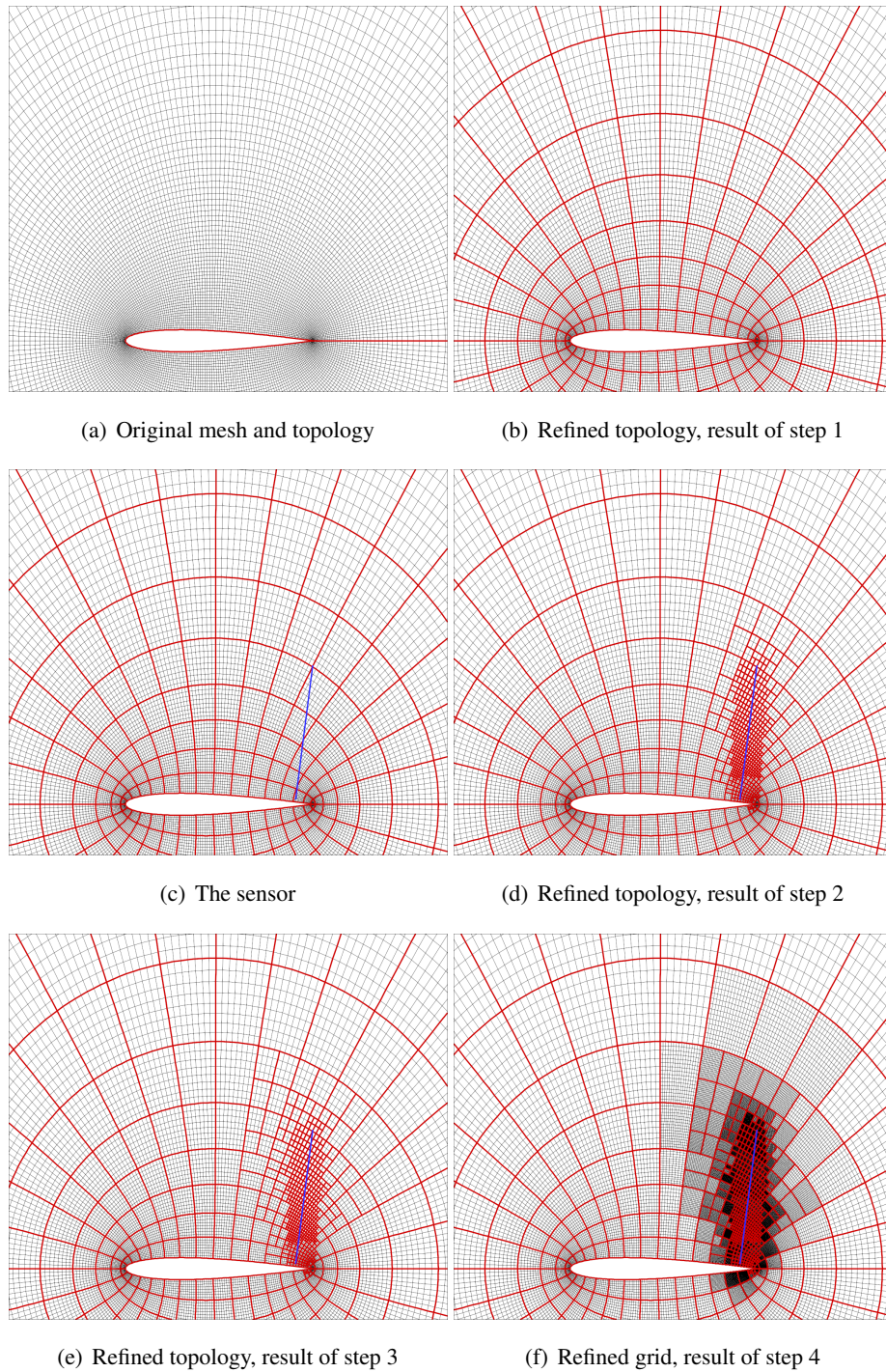


Fig. 1 Illustration of the grid generation algorithm. Block boundaries are shown in red; grid lines in black; the line segment used in the sensor is shown in blue.

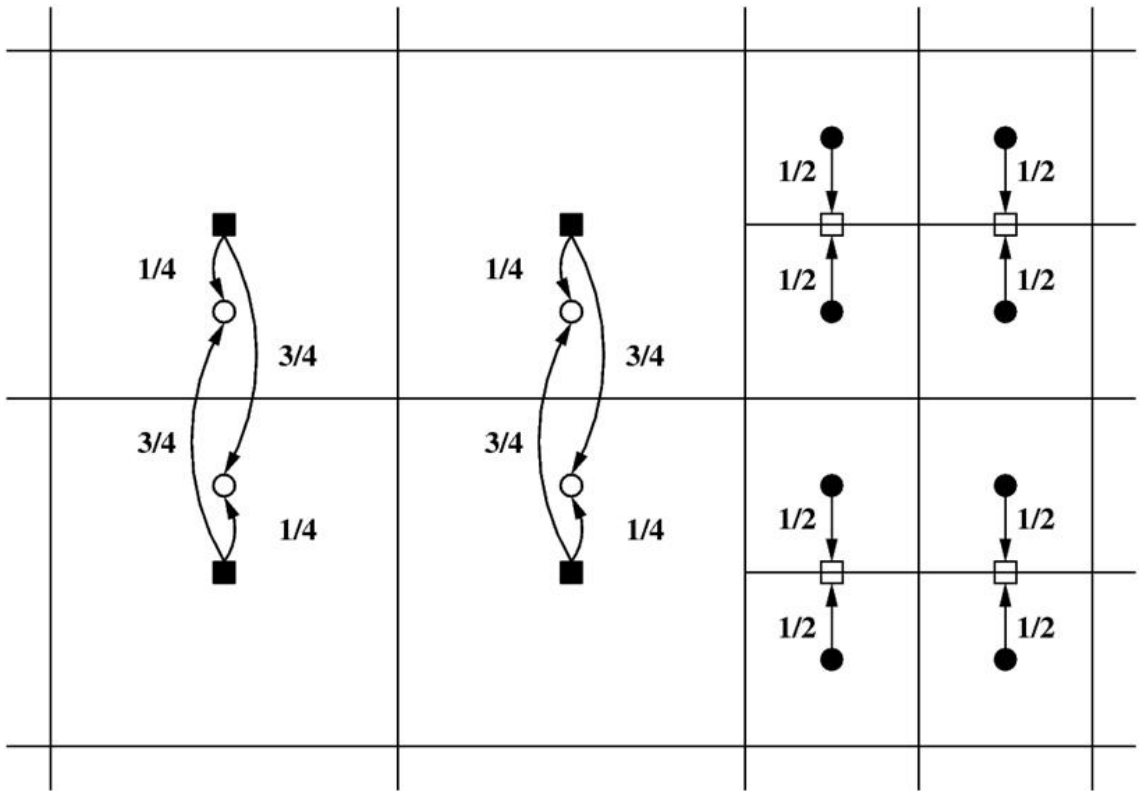
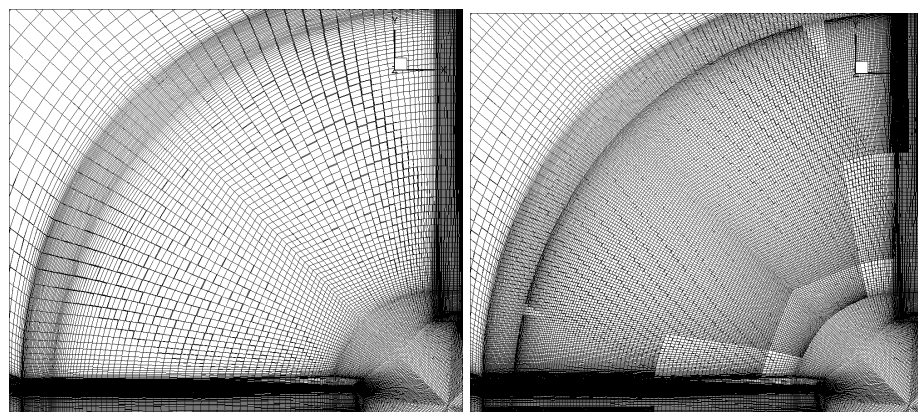


Fig. 2 Illustration of the interpolation algorithm at an irregular block interface



(a) Original mesh

(b) Refined mesh

Fig. 3 Original and refined mesh for the BO105 rotor at a horizontal plane through the hub.

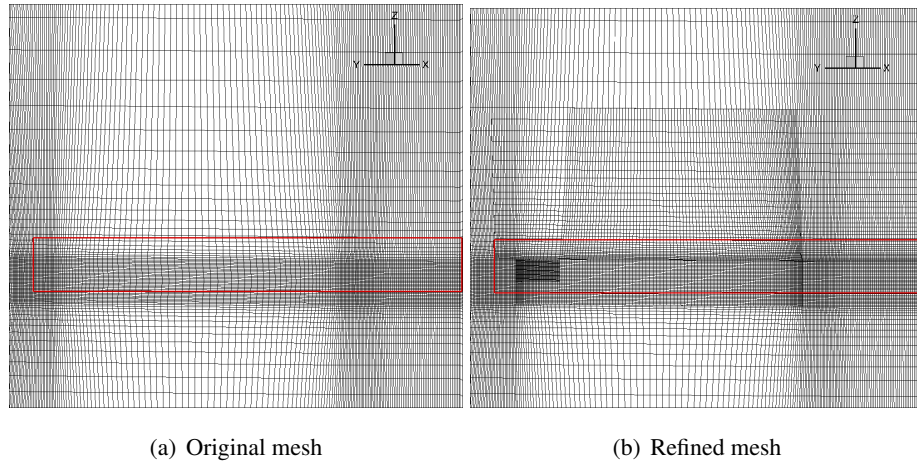


Fig. 4 Original and refined mesh for the BO105 rotor at a vertical plane between two blades. The refinement region is within the red rectangle.

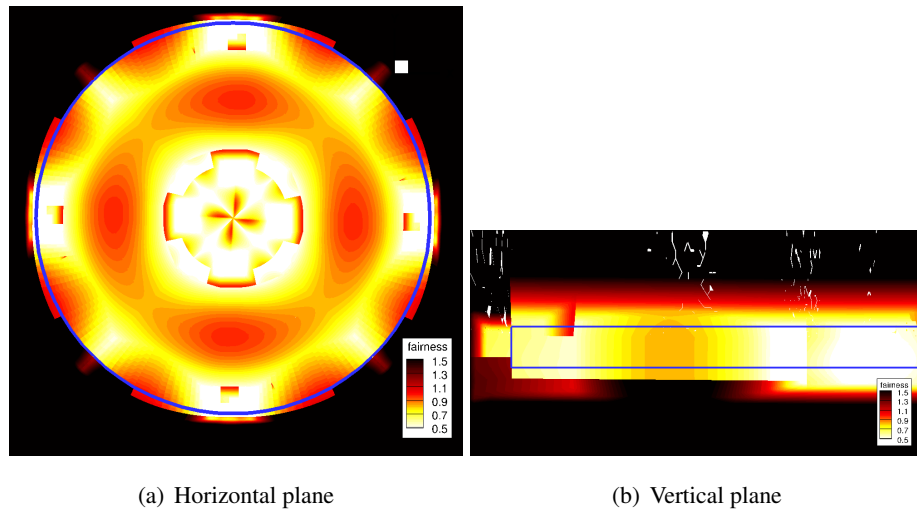


Fig. 5 Ratio of the maximum mesh width in a cell over the target mesh width in the same two planes as in the previous figures. The refinement region is shown in blue.

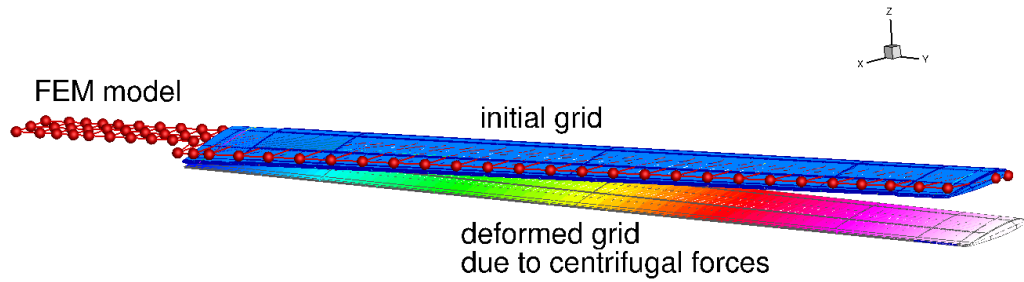


Fig. 6 Overview of the initial grid of the blade and deformed grid due to centrifugal force, about which the linearisation of the deformation is defined.

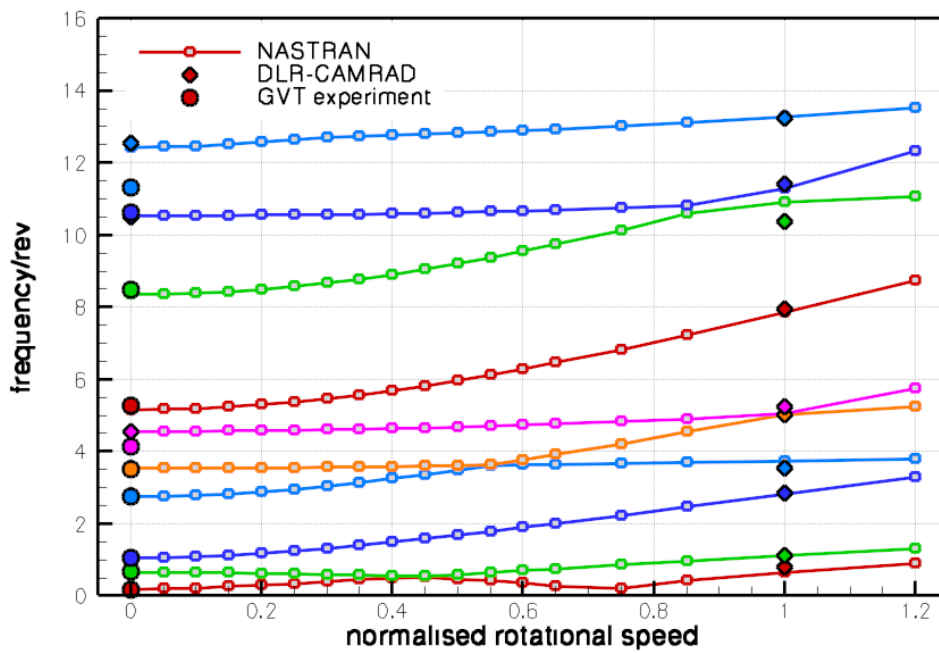


Fig. 7 Campbell diagram of the blade showing the influence of the rotational speed to the natural frequencies of the blade. The normalised rotational speed on the horizontal axis is normalised by the rotational speed of the HART-II experiment. Measured frequencies at zero rotational speed (GVT; coloured circles with black outline) and computed frequencies using CAMRAD (DLR-CAMRAD; coloured diamonds with black outline) at the reference rotational speed are taken from Ref. 7.

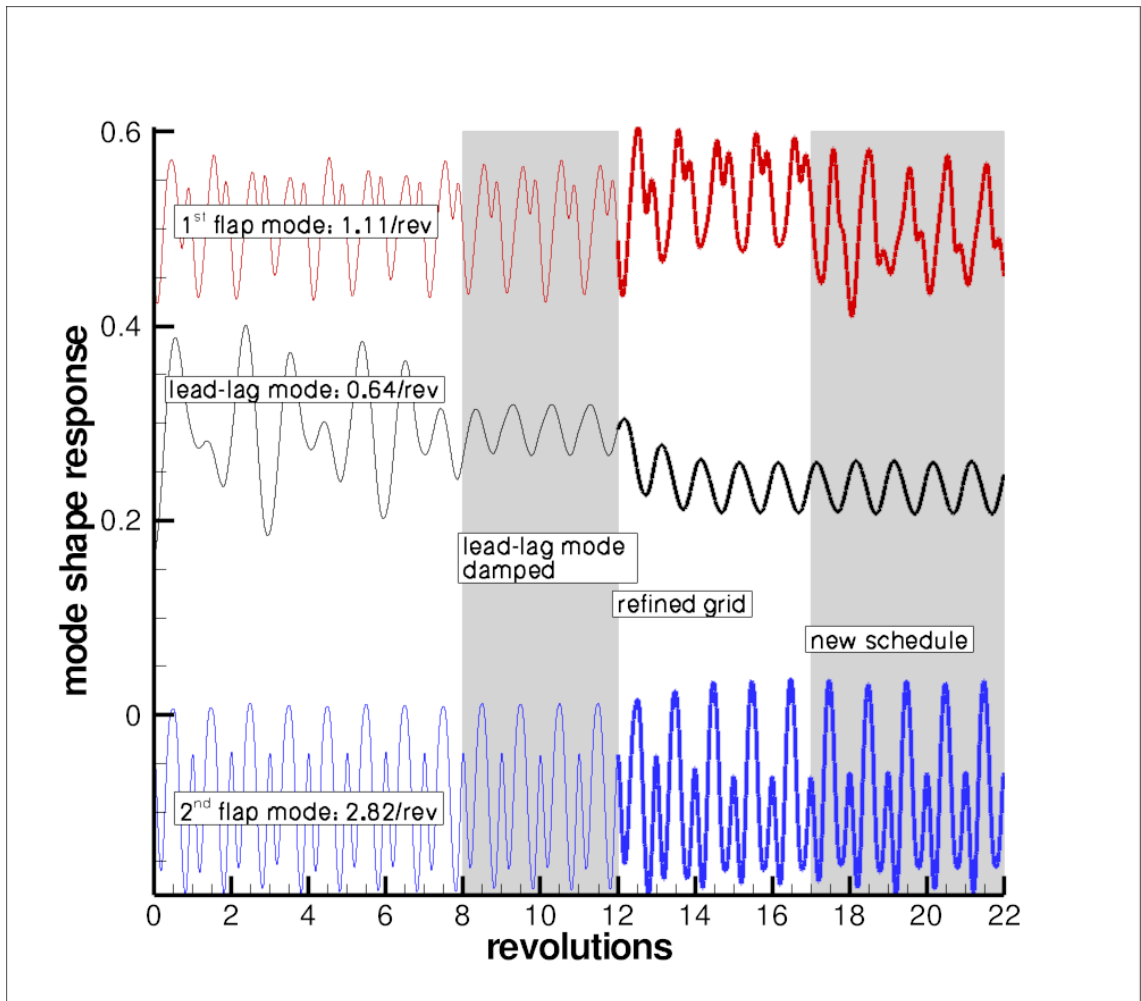


Fig. 8 The response of the first three modes for the simulations on original and refined meshes.

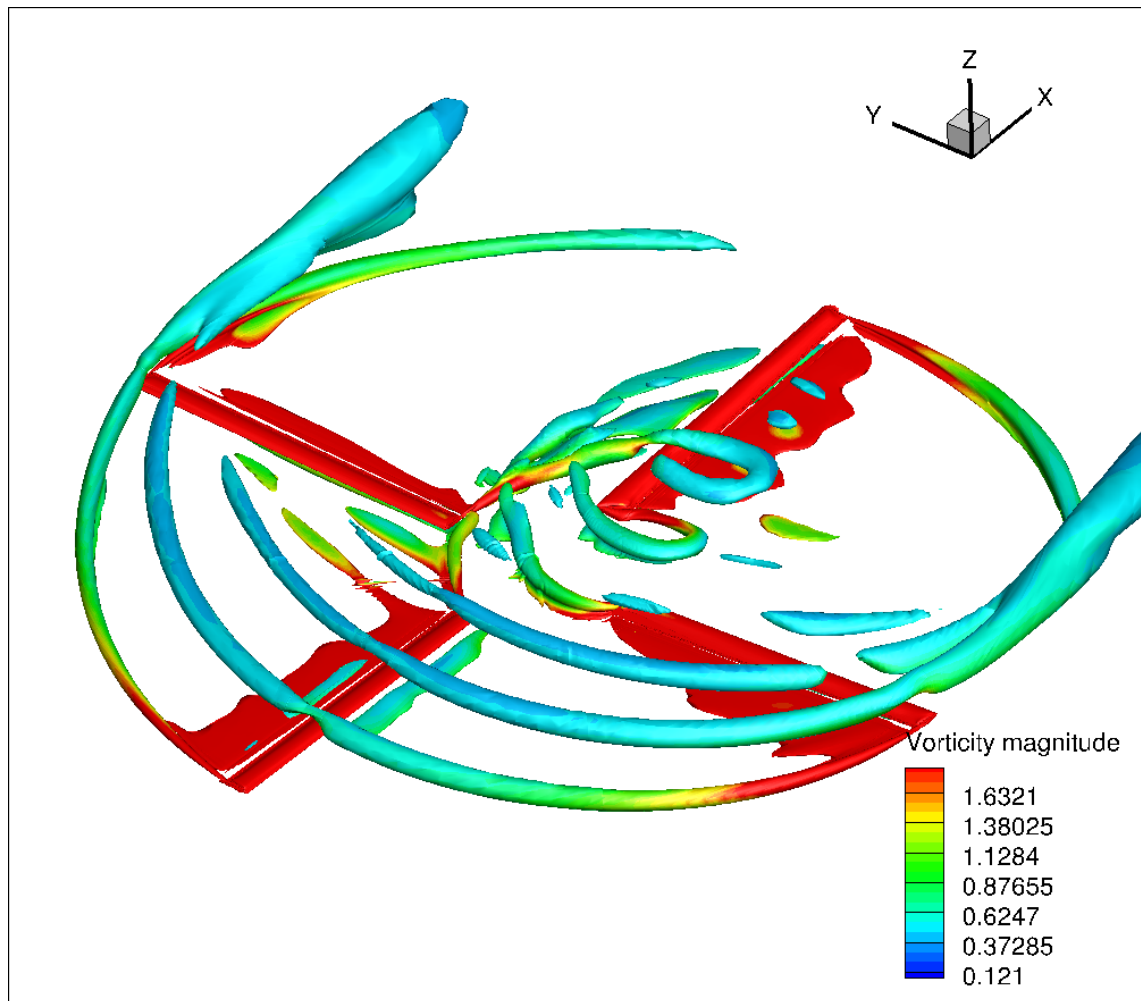


Fig. 9 Instantaneous iso-contour of the Q-criterion (blade at 0° azimuth) coloured with vorticity magnitude for the original mesh. Advancing side of the rotor is on the top-left side of the figure (positive y), retreating on the bottom-right side (negative y).

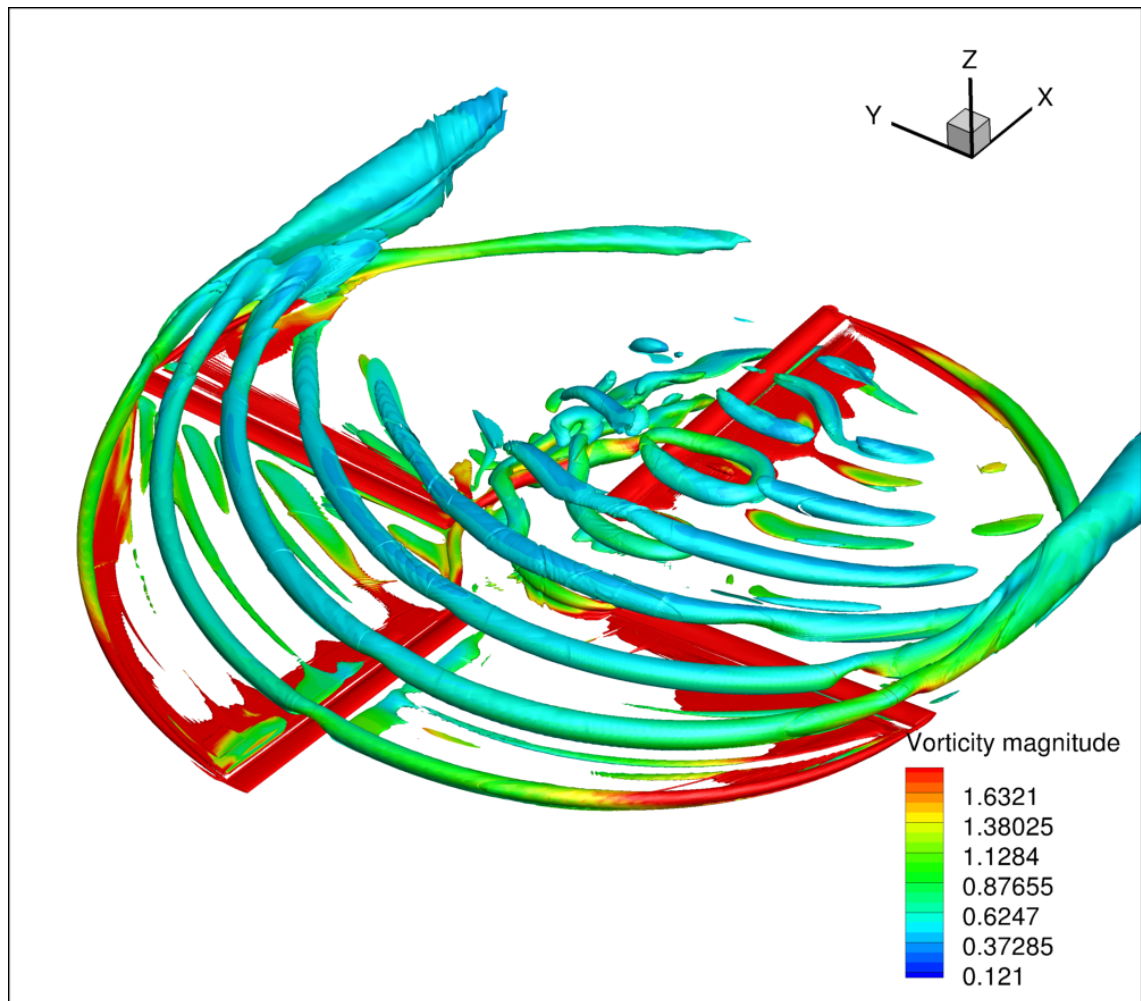


Fig. 10 Instantaneous iso-contour of the Q-criterion (blade at 0° azimuth) coloured with vorticity magnitude for the refined mesh. Advancing side of the rotor is on the top-left side of the figure (positive y), retreating on the bottom-right side (negative y).

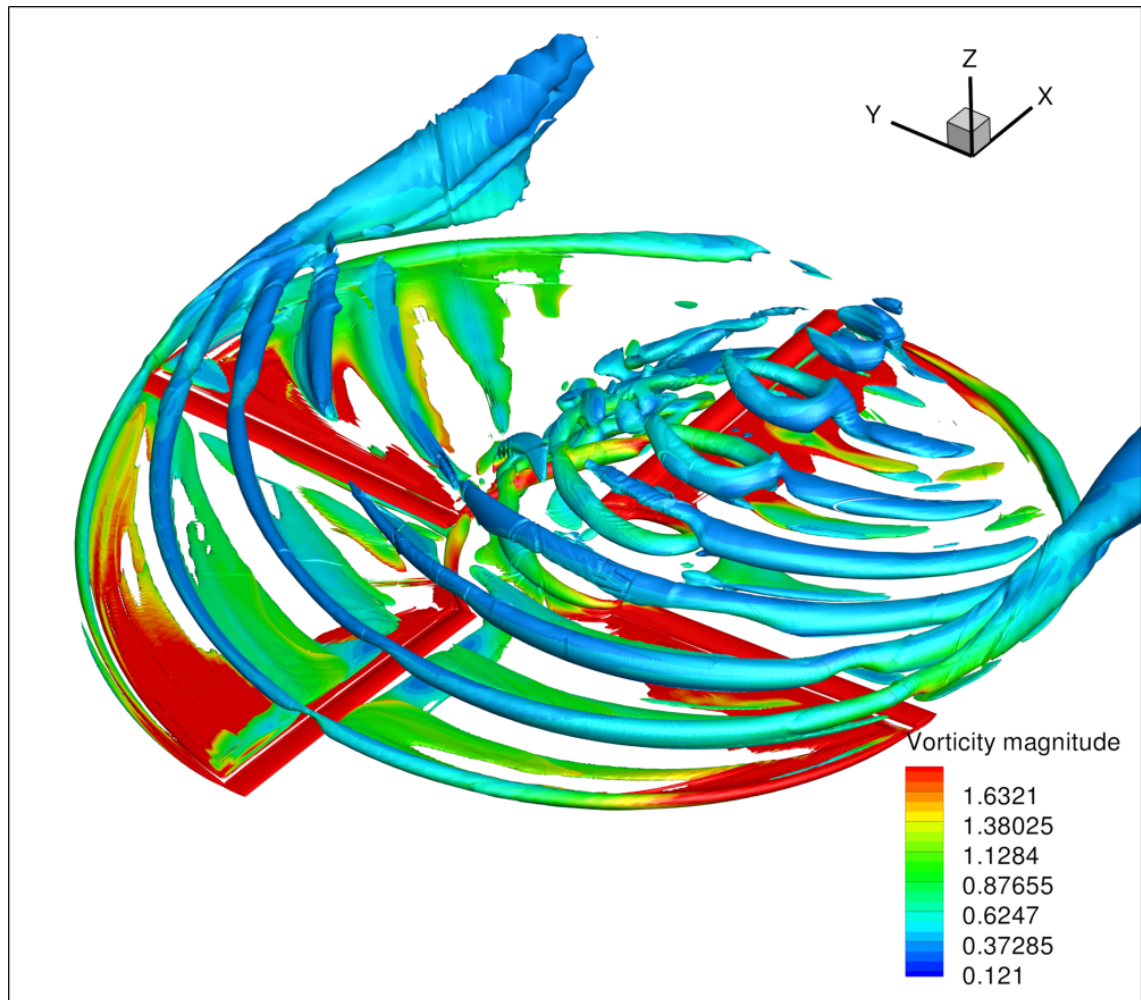


Fig. 11 Instantaneous iso-contour of the Q-criterion (blade at 0° azimuth) coloured with vorticity magnitude for the refined mesh and flexible blades. Advancing side of the rotor is on the top-left side of the figure (positive y), retreating on the bottom-right side (negative y).

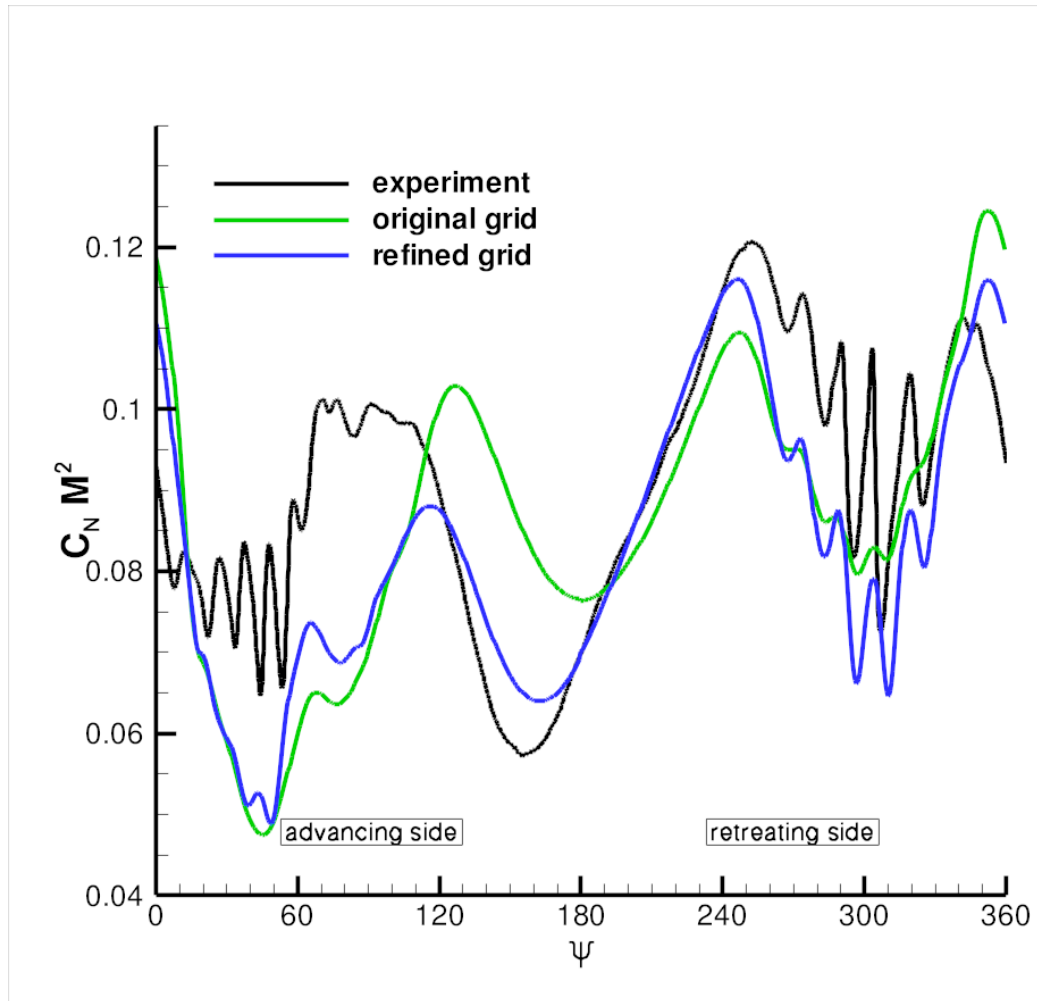


Fig. 12 Vertical force coefficient at 87% span for the simulations with flexible blades. Black line: experiment; green line: original grid; blue line: refined grid.

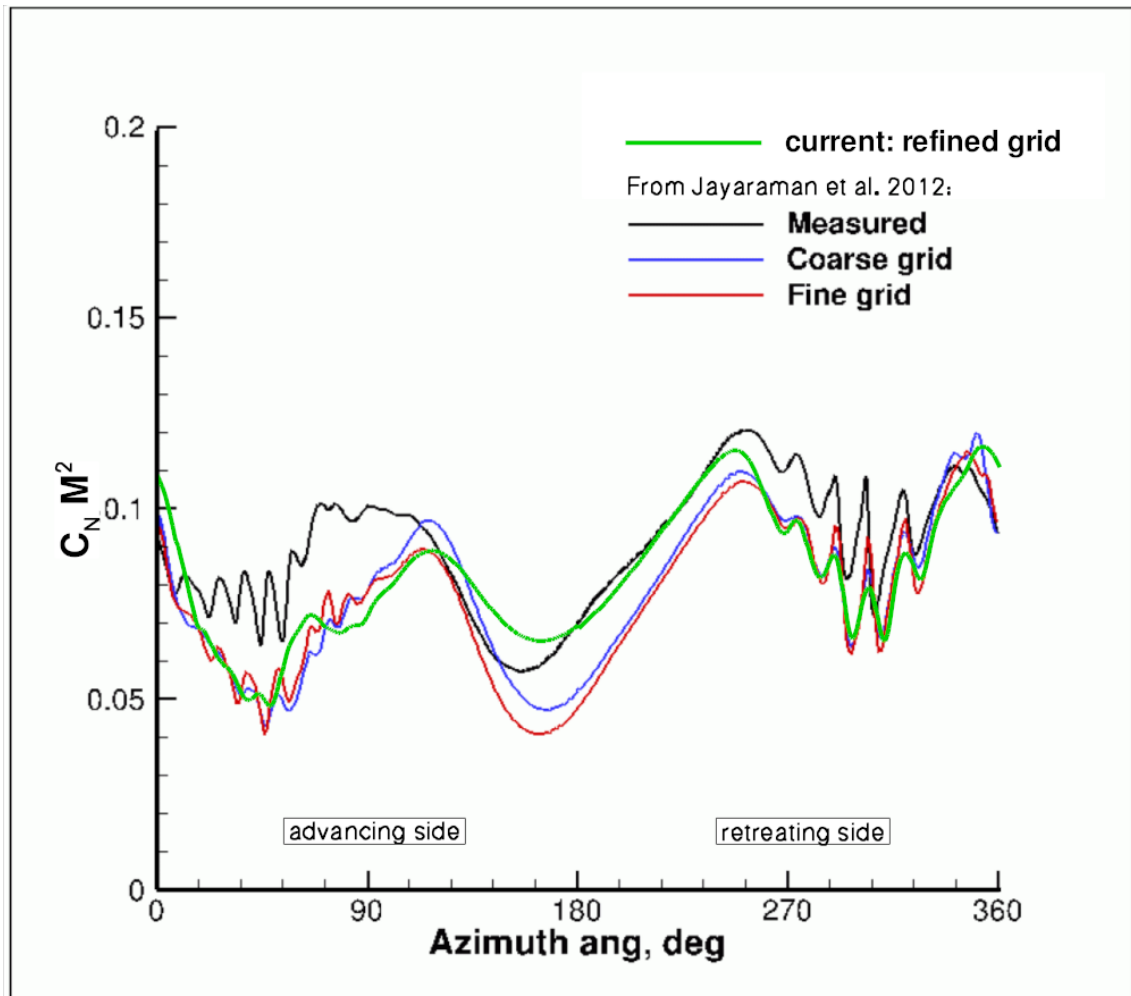


Fig. 13 Vertical force coefficient at 87% span for the simulations with flexible blades. Black line: experiment; green line: refined grid; red and blue line: results from Jayaraman et al. (Ref. 2).